PAPER

Check for updates

Molecular conformation modulating luminescence switching between delayed fluorescence and room-temperature phosphorescence†

Yating Wen,[a] Shengbing Xiao,[a] Haichao Liu,*[a] Xuzhou Tian,[a] Jianbo De,[b] Tong Lu,[a] Zhiqiang Yang,[a] Deyue Zou,[cd] Ying Lv, [c] Shi-Tong Zhang,[a] Qing Su [e] and Bing Yang *[a]

A new pure organic donor–acceptor molecule, (4-chlorophenyl)(5*H*-dibenzo[*b,f*]azepin-5-yl)methanone (IS-CBZ), was designed and synthesized, which demonstrates near ultraviolet (NUV) delayed fluorescence (DF) and dual emission of NUV DF and yellow room-temperature phosphorescence (RTP) in two crystals (B-crystal and Y-crystal), respectively. These two kinds of luminescence (DF and RTP) can be reversibly switched by external stimuli, such as grinding and heating/fuming, accompanied by reversible phase transition between two crystalline states. The experimental and theoretical studies reveal that this switchable luminescence between DF and RTP originates from a single-molecule conformational change in different molecular packings, mainly involving the twist angle (θ) between the donor and acceptor units. This θ fundamentally modulates the energy difference between the lowest singlet state (S_1) and the high-lying triplet state (T_2), ΔE_{S1-T2}, which determines the luminescence switching between DF and RTP. This work not only provides a new donor–acceptor architecture for pure organic multifunctional materials with mechanochromic luminescence (MCL) and mechanoluminescence (ML) properties, but also suggests a novel strategy to design stimuli-responsive materials with a unique luminescence switching between DF and RTP by tuning T_2.

Introduction

Pure organic luminescence materials have become a research focus, which is not only due to their rich chemical structures and low cost, but also due to the diversity of luminescence properties and potential applications (*e.g.*, organic light-emitting diodes, sensors/detectors, memory/storage, information security and biological imaging).[1–8] In terms of luminescence mechanism, room-temperature phosphorescence (RTP),[9,10] delayed fluorescence originating from triplet–triplet annihilation (TTA)[11,12] and thermally activated delayed fluorescence

(TADF),[13,14] as well as "hot-exciton",[15,16] are aimed to make full use of triplet state energy, which is the most important scientific issue when utilizing pure organic luminescence materials. Differently, the achievement of these luminescence mechanisms depends on the distinct energy level distribution: RTP is commonly harvested along with a large energy level difference between the lowest triplet state (T_1) and lowest singlet state (S_1), by the direct radiation of the T_1 state back to the ground state (S_0) after the intersystem crossing (ISC) process to populate triplet states; the TTA process by molecular collision to transform the triplet states into the radiative higher-energy singlet states is favorable when the double energy of the T_1 state is larger than that of the S_1 state; the TADF process that is usually achieved by the up-conversion of triplet states *via* the reverse intersystem crossing (RISC) process along the path from the T_1 to S_1 state prefers a small energy level difference between the T_1 and S_1 states; the "hot exciton" channels for achievement of the radiative singlet states can be constructed to obtain the RISC at high energy levels by the resonant alignment of the $T_m(m \geq 2)$ and $S_n(n \geq 1)$ energy levels. From the description above, the dual emission originating from a combination of two luminescence mechanisms among them, is attractive in the study of photophysical foundation and stimuli-responsive luminescence switching.

[a] *State Key Laboratory of Supramolecular Structure and Materials, College of Chemistry, Jilin University, Changchun 130012, P. R. China. E-mail: hcliu@jlu.edu.cn, yangbing@jlu.edu.cn*

[b] *Beijing Key Laboratory for Optical Materials and Photonic Devices, Department of Chemistry, Capital Normal University, Beijing 300072, P. R. China*

[c] *State Key Laboratory of Luminescence and Applications, Changchun Institute of Optics, Fine Mechanics and Physics, Chinese Academy of Sciences, Changchun 130033, P. R. China*

[d] *University of Chinese Academy of Sciences, Beijing 100049, P. R. China*

[e] *College of Chemistry, Jilin University, Changchun 130012, P. R. China*

† Electronic supplementary information (ESI) available. CCDC 1967882 and 1967881. For ESI and crystallographic data in CIF or other electronic format see DOI: 10.1039/d1tc02265b

This journal is © The Royal Society of Chemistry 2021

J. Mater. Chem. C, 2021, **9**, 17511–17517 | 17511

However, it is difficult and challenging to integrate these luminescence mechanisms into a molecule because, in the case of only considering two excited states T_1 and S_1, the intrinsic distribution of energy level cannot be satisfied simultaneously, letting alone the uncontrolled competition between ISC and RISC processes in a complex solid-state environment.

It seems to be possible that from these luminescence mechanisms mentioned above, the RTP and TTA-based DF can be simultaneously realized in a single-component material due to the similar distribution of the energy levels,[17–21] although a few pure organic donor–acceptor (D–A) molecules have been reported with dual emissions of RTP and TADF at room temperature (RT).[22–28] As regards the dual emission of RTP and DF, the structure–property relationship remains unclear and deserves a further exploration of the accurate adjustment and control of the excited state. Moreover, a reversible luminescence switching could be further expected to achieve between RTP and DF for a pure organic single-component material, if the excited state becomes precisely tunable in energy and excitation characteristics. But so far, the luminescence switching between the RTP and DF by an external stimuli has been rarely reported.

In this work, we developed a new pure organic D–A molecule, (4-chlorophenyl)(5*H*-dibenzo[*b*, *f*]azepin-5-yl)methanone (IS-CBZ, Fig. 1a), in which the iminostilbene (IS) moiety is used as a donor and the *p*-chlorobenzoyl group serves as an acceptor. We found in experiments that two crystals of IS-CBZ were obtained with distinct photophysical properties, including a needle-like B-crystal and a bulk Y-crystal (Fig. 1). The B-crystal demonstrates a rare near ultraviolet (NUV) DF emission with a high photoluminescence quantum yield (PLQY), together with a unique NUV mechanoluminescence (ML). As a comparison, the Y-crystal exhibited an RTP-dominated dual emission along with DF, which is exactly as we desired in a pure organic material. The IS-CBZ molecules in two crystals possess the same energy level characteristics of $2E_{T1} \geq E_{S1}$, enabling the occurrence of a TTA process. And these distinct photophysical properties of two crystals originate from a key structural difference, the twist angle (θ) between the donor and acceptor units, which mainly modulates the T_2 state character. A small θ in the B-crystal leads

to a small ΔE_{S1-T2}, which is beneficial to the only TTA-caused DF emission in the B-crystal. When the θ increases in the Y-crystal, the ΔE_{S1-T2} is greatly enlarged and ΔE_{T1-T2} is remarkably reduced by the stabilization of the T_2 state, resulting in the predominance of RTP along with the decrease of DF relative to that of the B-crystal. More importantly, the T_2 state was verified experimentally using the temperature-dependent photoluminescence (PL) spectra. A reversible mechanochromic luminescence (MCL) was observed between DF and RTP by grinding and fuming/heating treatments, corresponding to a rare crystal-to-crystal phase transition between the B-crystal and Y-crystal. To the best of our knowledge, IS-CBZ is novel as a pure organic multifunctional material with simultaneous ML and MCL properties. This work provides a novel strategy to design stimuli-responsive materials with a unique luminescence switching between DF and RTP by regulating the high-lying triplet excited state (T_2).

Results and discussion

The pure product of IS-CBZ was obtained through a series of steps, such as synthesis, separation and purification (Scheme S1, ESI†). First of all, its single-molecule photophysical properties were characterized in dilute solutions of different solvent polarities. IS-CBZ shows a structureless absorption band around 280 nm, and it hardly changes with the increasing solvent polarity. From the PL spectra (Fig. S1, ESI†), IS-CBZ exhibits dual fluorescence (peaks at ~400 and ~600 nm, respectively) in low-polarity solvents (*e.g.*, *n*-hexane), corresponding to the emission from locally-excited (LE) and charge-transfer (CT) states, respectively. Differently, a single emission band in the short-wavelength region was observed in high-polarity solvents (*e.g.*, acetonitrile), indicating the quenched CT emission peak at 600 nm due to the excessive energy stabilization induced by the strongly polar solvent. For the solid-state properties, two polymorphic crystals were achieved by different methods: a B-crystal from sublimation and a Y-crystal from slow evaporation of dichloromethane solution. As shown in Fig. 2a, the B-crystal of IS-CBZ at RT exhibits a very rare highly efficient NUV emission, featured with a PLQY of 75.2%, a peak wavelength at λ_{max} = 398 nm and CIE coordinates of (0.16, 0.06). The transient PL decay of the B-crystal identifies two emission components: prompt fluorescence (PF) with a lifetime of 4.5 ns and DF with a lifetime of 842.0 µs (Fig. 2b). Meanwhile, a NUV ML phenomenon was also found for the B-crystal by simply scraping the crystal. As shown in Fig. 2c, bright NUV ML can be observed obviously with almost the same spectral profile as the PL emission of the B-crystal. This is a rare DF sample showing ML properties. As a comparison, the Y-crystal exhibits a slightly yellow emission with a low PLQY of 8.1% (Table S1, ESI†), which consists of two emission bands: a weak emission band peaking at ~398 nm and a strong emission band peaking at 546 nm in Fig. 2d. The transient PL decay of the Y-crystal at 398 nm shows a prompt lifetime of 3.3 ns and a delayed component of 808.3 µs (Fig. 2e).
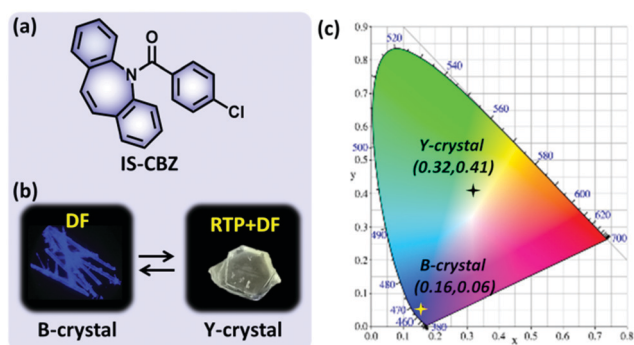

Fig. 1 (a) Molecular structure of IS-CBZ; (b) luminescence images of IS-CBZ for the B-crystal and Y-crystal; (c) CIE 1931 coordinates of IS-CBZ in different crystals.

17512 | *J. Mater. Chem. C*, 2021, **9**, 17511–17517

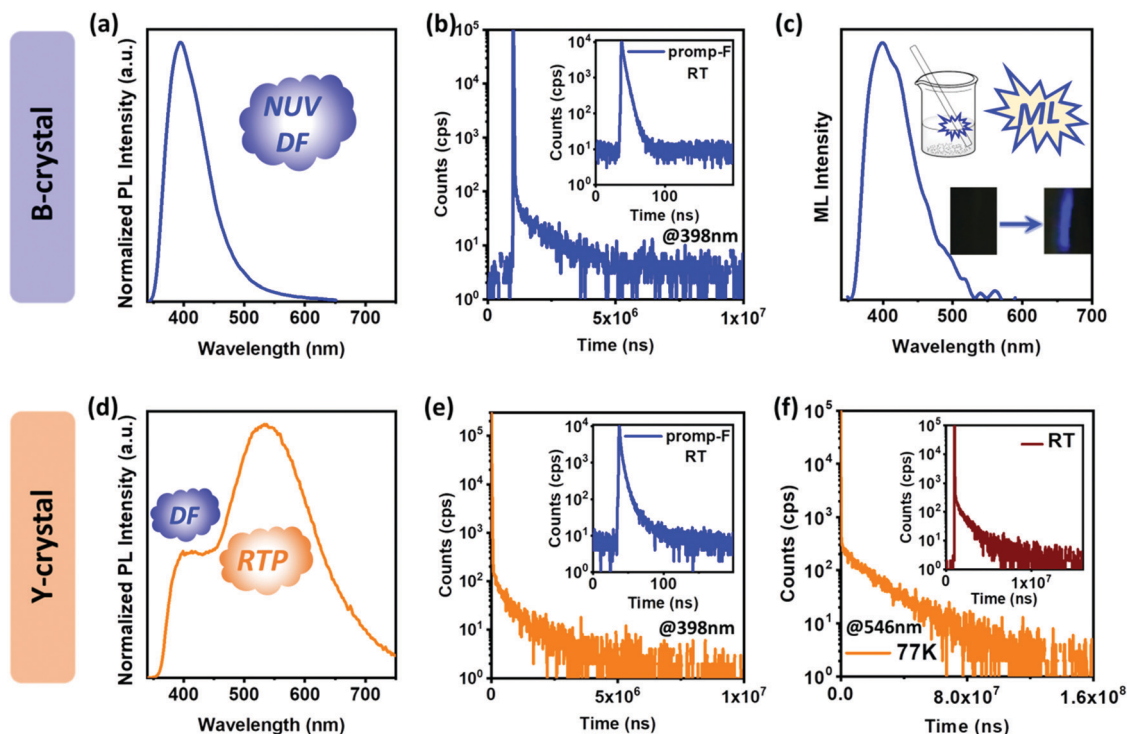This journal is © The Royal Society of Chemistry 2021

Fig. 2 (a) PL spectra of IS-CBZ for the B-crystal; (b) transient PL decay for the B-crystal at 398 nm at RT; (c) ML spectra of IS-CBZ for the B-crystal; (d) PL spectra of IS-CBZ for the Y-crystal; (e) transient PL decay for the Y-crystal at 398 nm at RT; (f) transient PL decay for the Y-crystal at 546 nm at 77 K (inset: at RT).

Thus, both the B-crystal and Y-crystal have the same NUV emission, arising from the joint contribution of PF and DF in nature. Differently, the transient PL decay of the Y-crystal at 546 nm shows a persistent lifetime of about 21.0 ms at 77 K and 2.1 ms at RT, corresponding to a typical RTP emission in Fig. 2f. Unlike the B-crystal, the Y-crystal displays an unusual dual emission of DF and RTP in a pure organic material, whereas the RTP dominates the whole emission and ML is completely absent in the Y-crystal. As for the DF, it may result from one of the TTA and TADF, which will be discussed in detail in the following experiments.

In order to understand the above distinct photophysical properties, the crystal structures of the B-crystal and Y-crystal were resolved by single crystal X-ray diffraction (XRD) for the purpose of comparison. In Fig. 3, IS-CBZ demonstrates an obviously twisted structure of single molecule in both the B-crystal and Y-crystal, including the folding conformation of the IS unit itself and two major twist angles between three groups of IS, carbonyl and chlorobenzene (Fig. S2 and Table S2, ESI†). In particular, the twist angle (θ) between the IS and acceptor groups contributes to the main difference of molecular conformation between the B-crystal and Y-crystal, and they are $-9.55°$ and $-18.93°$, respectively. Such a significant difference in the twist angle should be due to the structural nature that leads to the distinct photophysical properties between the B-crystal and Y-crystal. Due to the highly twisted molecular structure, there is no intermolecular π–π interaction for long-range ordered molecular alignment in two crystals. As a matter of fact, there are
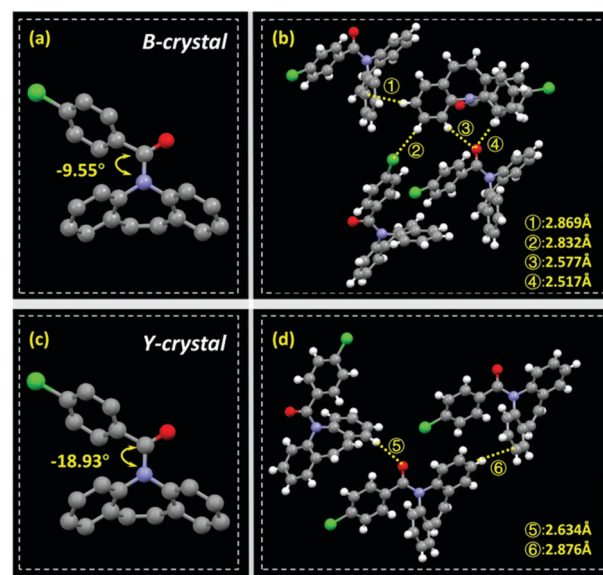

Fig. 3 Different molecular conformations in (a) B-crystal and (c) Y-crystal; intermolecular interactions in (b) B-crystal and (d) Y-crystal.

only a few kinds of weak hydrogen bonds in the B-crystal and Y-crystal, such as C–H···π (2.869 Å), C–H···Cl (2.832 Å) and double C–H···O (2.517 Å, 2.577 Å) in the B-crystal, and C–H···π (2.876 Å) and C–H···O (2.634 Å) in the Y-crystal. As a comparison, the B-crystal presents relatively stronger intermolecular

This journal is © The Royal Society of Chemistry 2021

J. Mater. Chem. C, 2021, 9, 17511–17517 | 17513

interactions than the Y-crystal, which may be responsible for the rare NUV ML by scraping the B-crystal.[29–31]

Based on the difference in the crystal structure, theoretical and experimental investigations were further carried out to clarify their photophysical mechanisms between the B-crystal and Y-crystal. First, the S_1 and T_1 energies of the Y-crystal can be experimentally determined due to the dual emission of DF and RTP, corresponding to E_{S1} = 3.12 eV and E_{T1} = 2.27 eV, respectively. Thus, a large energy gap ΔE_{S1-T1} was estimated to be 0.85 eV between S_1 and T_1 states, which is surely impossible for an up-conversion to produce the TADF by RISC ($T_1 \rightarrow S_1$).[17] However, from the perspective of the energy level difference between the T_1 and S_1 states, the TTA process is also favorable because $2E_{T1}$ is larger than E_{S1}.[11] In order to further distinguish the TADF and TTA, we collected the PL spectra of samples under different excitation powers, and then the double-logarithmic relationship between the excitation power and the PL intensity was fitted. As shown in Fig. S3 (ESI†), the B-crystal and Y-crystal of IS-CBZ show a slope between 1 and 2, which indicates the possible presence of TTA.[32–34] The TTA-based DF shows almost the same emission peak as that of PF, revealing the identical S_1 irradiation of DF and PF (Fig. S4, ESI†). If the short-wavelength emission peak at 398 nm of the Y-crystal of IS-CBZ is ascribed to the TTA-based DF, another problem of why the B-crystal shows only DF but the Y-crystal exhibits the dual emission of RTP and DF needs to be considered. For this problem, sometimes the balance between these two photophysical processes can be established by introducing an upper triplet state (such as T_2).[22] To confirm the participation of the T_2 state, the temperature-dependent PL spectra were recorded from 80 K to 320 K for the Y-crystal. Once at 80 K, a new emission band appears around 438 nm with a long-lived lifetime of 71.1 ms (Fig. 4 and Fig. S5, ESI†), which is neither a DF emission peaking at 398 nm nor phosphorescence emission from the T_1 state peaking at 546 nm with a lifetime of 21.0 ms (Table S3, ESI†). The temperature-dependent PL spectra and the delayed PL spectra further demonstrate that this new emission band should result from the high-lying T_2 excited state (Fig. 4b and d, Fig. S6 and S7, ESI†). Accordingly, ΔE_{S1-T2} = 0.29 eV was estimated for the Y-crystal. At RT, the T_2 state is nonradiative, probably due to the temperature-accelerated quenching through two pathways of consumption: RISC ($T_2 \rightarrow S_1$) and internal conversion (IC) ($T_2 \rightarrow T_1$). The luminescence process can be further understood when the T_1 states are populated abundantly through the ISC and then the IC. On the one hand, two migrating T_1 states may collide to generate the radiative S_1 state, i.e. TTA process;[11,12,35–37] on the other hand, the T_1 state may directly radiate to produce the RTP. Therefore, the Y-crystal shows a dual emission of DF and RTP.
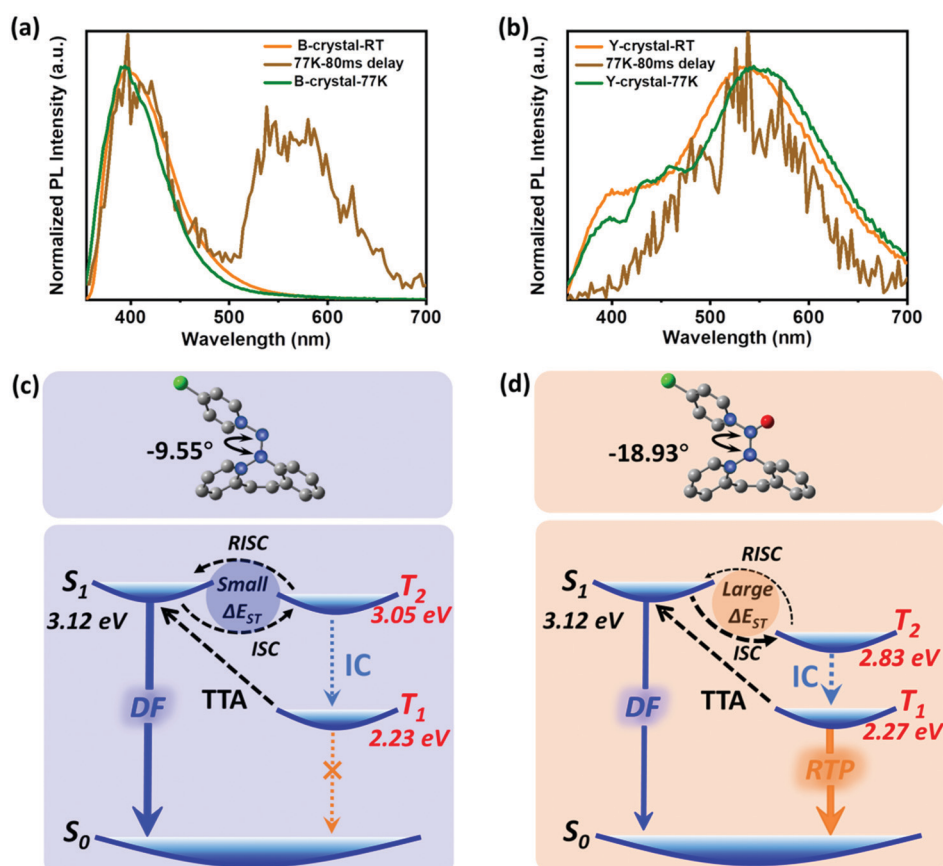

Fig. 4 PL spectra of the (a) B-crystal and (b) Y-crystal; mechanism for DF and RTP emissions in the (c) B-crystal and (d) Y-crystal, respectively.

Second, for the purpose of comparison, we tried to determine the energy levels of T_1 and S_1 states in the B-crystal. At RT, the B-crystal shows the same DF emission peak at 398 nm as that of the Y-crystal, indicative of their same S_1 state energy of $E_{S1} = 3.12$ eV, whereas the T_1 state cannot be determined due to the absence of RTP emission. Upon low temperature at 77 K, a new emission band of the B-crystal was observed around 556 nm ($E_{T1} = 2.23$ eV) after a long lifetime decay, corresponding to a phosphorescence emission of the T_1 state due to the suppressed nonradiation (Fig. 4a). For the B-crystal, a large energy gap $\Delta E_{S1-T1} = 0.89$ eV was obtained between the S_1 and T_1 states, which is also impossible for RISC ($T_1 \rightarrow S_1$) to generate TADF. Hence, it can be inferred that the DF of the B-crystal may also originate from the TTA process (Fig. S3, ESI†). Moreover, as for the B-crystal at 77 K, with an increasing delay time, the recorded PL spectra show a slightly red-shifted maximum to ~ 406 nm, which should be ascribed to the T_2 emission. Thus the T_2 state is very close to S_1 in energy (Fig. 4a and c, Fig. S7a and S7b, ESI†). The calculated ΔE_{S1-T2} is 0.07 eV and ΔE_{T1-T2} is 0.82 eV. According to the previous reports,[15,16,38,39] when the ΔE_{T1-T2} is large enough, the IC process from the T_2 to T_1 state can be suppressed. At this time, if ΔE_{S1-T2} is small enough, the RISC through the "hot exciton" channel of $T_2 \rightarrow S_1$ is very fast, theoretically not resulting in the microsecond lifetime like those of the B-crystal and Y-crystal in this work. Therefore, the DF should result from the TTA process. Through a comparison, the B-crystal possesses a smaller ΔE_{S1-T2} and a larger ΔE_{T1-T2} than those of the Y-crystal, corresponding to a much faster RISC ($T_2 \rightarrow S_1$) rate and a slower IC ($T_2 \rightarrow T_1$) rate in the B-crystal than those in the Y-crystal.[40] Relative to the Y-crystal, in the B-crystal, the T_1 state may be generated poorly so that the T_1 radiation cannot be comparable with the TTA process, which may be favorable to the exclusive S_1 radiation instead of the introduction of the RTP.

Third, based on the different molecular conformations between the B-crystal and Y-crystal, the time-dependent density functional theory (TD-DFT) with Tamm–Dancoff approximation was performed to calculate the excited state properties at the level of B3LYP/6-31G (d, p). Although they are two different conformers, they show very similar energy level distribution of excited states, such as large ΔE_{S1-T1} and ΔE_{T1-T2} as well as a small ΔE_{S1-T2}, which are very consistent with the experimental data (Fig. 4c, d and Fig. S8, ESI†). Theoretical energy levels as a function of θ between the donor and acceptor demonstrate that the ΔE_{S1-T2} shows a roughly shrinking trend as the θ decreases (Fig. S9, ESI†). Exactly, the IS-CBZ molecule has a larger θ in the Y-crystal than that in the B-crystal, leading to a relatively larger ΔE_{S1-T2} than that in the B-crystal. This large ΔE_{S1-T2} reduces the RISC rate, and facilitates the generation of more triplet excitons for RTP occurrence. Furthermore, the natural transition orbitals (NTOs) were calculated to identify the excited state character for better understanding of their photophysical nature (Fig. S10, ESI†). For S_1 and T_1 states, both hole and electron wave functions are mainly localized on the IS unit, which indicates an identical LE state character to the IS, resulting in a similar large ΔE_{S1-T1} in the B-conformer and Y-conformer (Fig. S10 and S11, ESI†). Due to the different conformers (the twist angle θ), the T_2 state in the B-crystal demonstrates a hybridized local and charge-transfer (HLCT) character between the LE state of the p-chlorobenzoyl acceptor unit and the CT state from the IS donor to the acceptor in the B-conformer, while an obvious LE-dominated state of p-chlorobenzoyl exists for the Y-conformer. This difference of excited state character gives rise to the energy fluctuation of the T_2 state between the B-conformer and Y-conformer. Essentially, it is the change of twist angle θ that induces a tunable T_2 excited state in energy, which can work as a mediator state to control the generation of the T_1 state in the B-crystal and Y-crystal. Besides, the spin–orbit coupling (SOC) effect was also calculated between singlet and triplet manifolds by using the Beijing density function (BDF) program.[41,42] For both B-conformer and Y-conformer, the sizeable SOC coefficients were observed between S_1 and T_2 states, because of the different transition characters between (π, π^*) and (n, π^*) according to the El-Sayed rule (Fig. S10 and Table S4, ESI†).[43,44] In addition, more sizable SOC coefficients were found between S_2 and T_3/T_4 states (5.27/9.77 cm^{-1}) for the Y-conformer than those in the B-conformer (2.86/5.31 cm^{-1}), which facilitates the more favorable ISC process from the singlet to triplet states in the Y-crystal. Accordingly, this conformation-induced distinct luminescence determined by the twist angle between the donor and acceptor in the B-crystal and Y-crystal can be ascribed to a
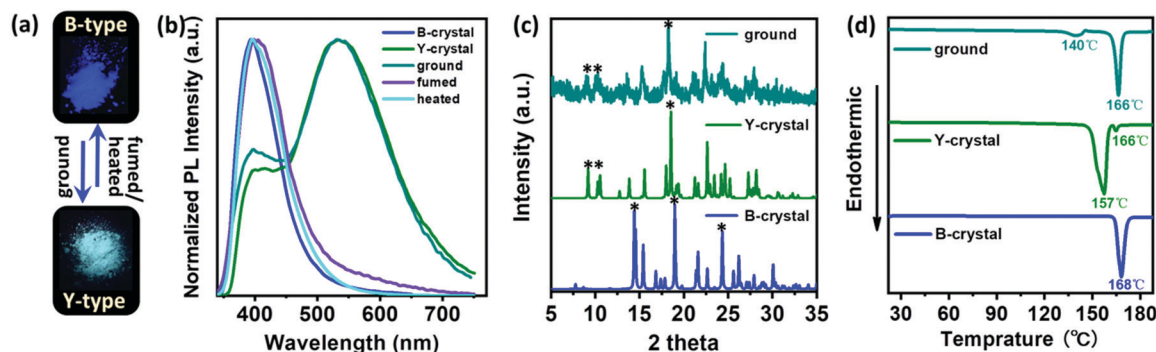

Fig. 5 (a) Luminescence images of the B-crystal and ground powder under illumination with UV light; (b) normalized PL spectra; (c) PXRD patterns; (d) DSC curves of the crystal-to-crystal phase transition.

This journal is © The Royal Society of Chemistry 2021

J. Mater. Chem. C, 2021, 9, 17511–17517 | 17515

tunable energy level of the high-lying T_2 excited state that acts as a mediator state to control the exciton population between the S_1 and T_1 states for DF and RTP-dominated emissions, respectively.

Inspired by the different polymorphs and PL spectra of two crystals, the phase transition between them was expected for reversible stimuli-responsive luminescence switching properties. Indeed, an interesting MCL was observed from blue to yellow–green color by grinding the B-crystal. Furthermore, the ground powder can reversibly return to blue color by fuming or by heating to 140 °C (Fig. 5a, b and Fig. S12, ESI†). To monitor the phase transition, the powder X-ray diffraction (PXRD) measurement was conducted before and after grinding. As shown in Fig. 5c, the XRD peaks of the B-crystal at 24.4°, 19.1° and 14.5° disappear after grinding, accompanied by the emergence of new diffraction peaks at 18.3°, 10.5° and 9.2° for the ground powder. The diffraction pattern of ground powder is in good agreement with the simulated one of the Y-crystal, indicating almost the same ordered molecular packing between the ground powder and Y-crystal. As a result, the grinding operation brings about a rare crystal-to-crystal phase transition from the B-crystal to the Y-crystal. This crystal-to-crystal phase transition was further confirmed by differential scanning calorimetry (DSC) measurements. As shown in Fig. 5d, the melting point (T_m) of the B-crystal was measured to be 168 °C. For ground powder, an endothermic peak arises at 140 °C, corresponding to the phase transition point. The ground powder shows the same T_m as that of the B-crystal, demonstrating a complete transformation from ground powder (Y-crystal-like) to the B-crystal. For the Y-crystal, an endothermic peak at 157 °C is assigned to the phase transition from the Y-crystal to B-crystal, followed by the endothermic T_m of the B-crystal. Overall, the DSC measurements reveal that the heating treatment results in a reversible phase transition from the Y-crystal to B-crystal.

Conclusions

In conclusion, we have developed a novel pure organic light-emitting material of IS-CBZ with an atypical donor–acceptor architecture, which exhibits versatile luminescence in two crystals: ML and NUV DF emission (λ = 398 nm and PLQY = 75.2%) in the B-crystal and RTP-dominated yellow emission in the Y-crystal. The luminescence switching (i.e. MCL) between DF and RTP can be reversibly conducted by some external stimuli (e.g., grinding and heating/fuming), accompanied by the reversible crystal-to-crystal transformation between two crystalline phases. The experimental and theoretical investigations disclose the nature for this luminescence switching between DF and RTP, which can be ascribed to a single-molecule conformational change in different molecular packings, especially for a twist angle change between the donor and acceptor moieties. When the twist angle is small, the only DF is achieved via the RISC ($T_2 \rightarrow S_1$) process due to a small ΔE_{S1-T2}. With the increasing twist angle, the energy level of the T_2 state gradually decreases and is away from the S_1 state, and thus RTP is harvested from the T_1 state through a more competitive IC

($T_2 \rightarrow T_1$) process relative to the slowing RISC ($T_2 \rightarrow S_1$) process. In addition, more effective ISC channels for triplet exciton generation are responsible for the RTP-dominated emission in the Y-crystal, because of more sizable SOC between singlet and triplet manifolds. As a result, we harvested a very rare pure organic multifunctional luminescence material with a variety of DF, RTP, ML, and MCL properties, arising from the molecular conformational dependence of the high-lying triplet state T_2 in essence. This work provides a new strategy for molecular design of stimuli-responsive luminescence switching materials with a unique luminescence switching between DF and RTP by the conformation-controlled T_2 state.

Conflicts of interest

There are no conflicts to declare.

Acknowledgements

Notes and references

1 C. W. Tang and S. A. VanSlyke, *Appl. Phys. Lett.*, 1987, **51**, 913–915.

2 M. A. Baldo, D. F. O'Brien, Y. You, A. Shoustikov, S. Sibley, M. E. Thompson and S. R. Forrest, *Nature*, 1998, **395**, 151–154.

3 H. Uoyama, K. Goushi, K. Shizu, H. Nomura and C. Adachi, *Nature*, 2012, **492**, 234–238.

4 Z. An, C. Zheng, Y. Tao, R. Chen, H. Shi, T. Chen, Z. Wang, H. Li, R. Deng, X. Liu and W. Huang, *Nat. Mater.*, 2015, **14**, 685–690.

5 J. Wu, B. Kwon, W. Liu, E. V. Anslyn, P. Wang and J. S. Kim, *Chem. Rev.*, 2015, **115**, 7893–7943.

6 X. Chen, F. Wang, J. Y. Hyun, T. Wei, J. Qiang, X. Ren, I. Shin and J. Yoon, *Chem. Soc. Rev.*, 2016, **45**, 2976–3016.

7 J. Chan, S. C. Dodani and C. J. Chang, *Nat. Chem.*, 2012, **4**, 973–984.

8 A. Gansaeuer, C. Kube, K. Daasbjerg, R. Sure, S. Grimme, G. D. Fianu, D. V. Sadasivam and R. A. Flowers II, *J. Am. Chem. Soc.*, 2014, **136**, 1663–1671.

9 W. Z. Yuan, X. Y. Shen, H. Zhao, J. W. Y. Lam, L. Tang, P. Lu, C. Wang, Y. Liu, Z. Wang, Q. Zheng, J. Z. Sun, Y. Ma and B. Z. Tang, *J. Phys. Chem. C*, 2010, **114**, 6090–6099.

10 L. Gu, H. Shi, L. Bian, M. Gu, K. Ling, X. Wang, H. Ma, S. Cai, W. Ning, L. Fu, H. Wang, S. Wang, Y. Gao, W. Yao, F. Huo, Y. Tao, Z. An, X. Liu and W. Huang, *Nat. Photonics*, 2019, **13**, 406–411.

11 T. Serevičius, R. Komskis, P. Adomėnas, O. Adomėnienė, G. Kreiza, V. Jankauskas, K. Kazlauskas, A. Miasojedovas,

17516 | *J. Mater. Chem. C*, 2021, **9**, 17511–17517

This journal is © The Royal Society of Chemistry 2021

V. Jankus, A. Monkman and S. Juršėnas, *J. Phys. Chem. C*, 2017, **121**, 8515–8524.

12 C.-J. Chiang, A. Kimyonok, M. K. Etherington, G. C. Griffiths, V. Jankus, F. Turksoy and A. P. Monkman, *Adv. Funct. Mater.*, 2013, **23**, 739–746.

13 H. Uoyama, K. Goushi, K. Shizu, H. Nomura and C. Adachi, *Nature*, 2012, **492**, 234–238.

14 Q. Zhang, B. Li, S. Huang, H. Nomura, H. Tanaka and C. Adachi, *Nat. Photonics*, 2014, **8**, 326–332.

15 Y. Pan, W. Li, S. Zhang, L. Yao, C. Gu, H. Xu, B. Yang and Y. Ma, *Adv. Opt. Mater.*, 2014, **2**, 510–515.

16 Y. Xu, X. Liang, X. Zhou, P. Yuan, J. Zhou, C. Wang, B. Li, D. Hu, X. Qiao, X. Jiang, L. Liu, S.-J. Su, D. Ma and Y. Ma, *Adv. Mater.*, 2019, **31**, 1807388.

17 L. Gu, H. Shi, C. Miao, Q. Wu, Z. Cheng, S. Cai, M. Gu, C. Ma, W. Yao, Y. Gao, Z. An and W. Huang, *J. Mater. Chem. C*, 2018, **6**, 226–233.

18 E. Hamzehpoor, C. Ruchlin, Y. Tao, J. E. Ramos-Sanchez, H. M. Titi, G. Cosa and D. F. Perepichka, *J. Phys. Chem. Lett.*, 2021, **12**, 6431–6438.

19 T. Zhang, X. Wang, Z. An, Z. Fang, Y. Zhang and W. Z. Yuan, *Chem. Phys. Chem.*, 2018, **19**, 2389–2396.

20 C. Sun, X. Ran, X. Wang, Z. Cheng, Q. Wu, S. Cai, L. Gu, N. Gan, H. Shi, Z. An, H. Shi and W. Huang, *J. Phys. Chem. Lett.*, 2018, **9**, 335–339.

21 S. Kuno, T. Kanamori, Z. Yijing, H. Ohtani and H. Yuasa, *ChemPhotoChem*, 2017, **1**, 102–106.

22 I. Bhattacharjee, N. Acharya, H. Bhatia and D. Ray, *J. Phys. Chem. Lett.*, 2018, **9**, 2733–2738.

23 I. Bhattacharjee, N. Acharya and D. Ray, *Chem. Commun.*, 2019, **55**, 1899–1902.

24 R. Pashazadeh, P. Pander, A. Bucinskas, P. J. Skabara, F. B. Dias and J. V. Grazulevicius, *Chem. Commun.*, 2018, **54**, 13857–13860.

25 J. Chen, T. Yu, E. Ubba, Z. Xie, Z. Yang, Y. Zhang, S. Liu, J. Xu, M. P. Aldred and Z. Chi, *Adv. Opt. Mater.*, 2019, **7**, 1801593.

26 L. Zhan, Z. Chen, S. Gong, Y. Xiang, F. Ni, X. Zeng, G. Xie and C. Yang, *Angew. Chem., Int. Ed.*, 2019, **58**, 17651–17655.

27 J.-X. Wang, Y.-G. Fang, C.-X. Li, L.-Y. Niu, W.-H. Fang, G. Cui and Q.-Z. Yang, *Angew. Chem., Int. Ed.*, 2020, **59**, 10032–10036.

28 Y. Wang, J. Yang, Y. Tian, M. Fang, Q. Liao, L. Wang, W. Hu, B. Z. Tang and Z. Li, *Chem. Sci.*, 2020, **11**, 833–838.

29 Y. Xie, J. Tu, T. Zhang, J. Wang, Z. Xie, Z. Chi, Q. Peng and Z. Li, *Chem. Commun.*, 2017, **53**, 11330–11333.

30 C. Wang, B. Xu, M. Li, Z. Chi, Y. Xie, Q. Li and Z. Li, *Mater. Horiz.*, 2016, **3**, 220–225.

31 J. Yang, J. Qin, P. Geng, J. Wang, M. Fang and Z. Li, *Angew. Chem., Int. Ed.*, 2018, **57**, 14174–14178.

32 A. Haefele, J. Blumhoff, R. S. Khnayzer and F. N. Castellano, *J. Phys. Chem. Lett.*, 2012, **3**, 299–303.

33 D. Hertela, H. Bässler, R. Guentner and U. Scherf, *J. Chem. Phys.*, 2001, **115**, 10007–10013.

34 R. Vadrucci, C. Weder and Y. C. Simon, *Mater. Horiz.*, 2015, **2**, 120–124.

35 T. W. Schmidt and F. N. Castellano, *J. Phys. Chem. Lett.*, 2014, **5**, 4062–4072.

36 C. Cao, G.-X. Yang, J.-H. Tan, D. Shen, W.-C. Chen, J.-X. Chen, J.-L. Liang, Z.-L. Zhu, S.-H. Liu, Q.-X. Tong and C.-S. Lee, *Mater. Today Energy*, 2021, **21**, 100727.

37 A. Köhler and H. Bässler, *Mater. Sci. Eng., R*, 2009, **66**, 71–109.

38 W. Li, Y. Pan, R. Xiao, Q. Peng, S. Zhang, D. Ma, F. Li, F. Shen, Y. Wang, B. Yang and Y. Ma, *Adv. Funct. Mater.*, 2013, **24**, 1609–1614.

39 L. Yao, S. Zhang, R. Wang, W. Li, F. Shen, B. Yang and Y. Ma, *Angew. Chem., Int. Ed.*, 2014, **53**, 2119.

40 Y. Im, M. Kim, Y. J. Cho, J.-A. Seo, K. S. Yook and J. Y. Lee, *Chem. Mater.*, 2017, **29**, 1946–1963.

41 Z. Li, Y. Xiao and W. Liu, *J. Chem. Phys.*, 2012, **137**, 154114.

42 Z. Li, Y. Xiao and W. Liu, *J. Chem. Phys.*, 2014, **141**, 054111.

43 A. M. El-Sayed, *J. Chem. Phys.*, 1963, **38**, 2834–2838.

44 A. M. El-Sayed, *J. Chem. Phys.*, 1963, **38**, 3032–3033.

This journal is © The Royal Society of Chemistry 2021

J. Mater. Chem. C, 2021, **9**, 17511–17517 | **17517**